

**The Physics and Properties of Free-Electron Lasers**

S. Krinsky  
National Synchrotron Light Source  
Brookhaven National Laboratory  
P.O. Box 5000  
Upton, NY, USA 11973-5000

June 2002

**National Synchrotron Light Source**

Brookhaven National Laboratory  
Operated by  
Brookhaven Science Associates  
Upton, NY 11973

Under Contract with the United States Department of Energy  
Contract Number DE-AC02-98CH10886

## **DISCLAIMER**

This report was prepared as an account of work sponsored by an agency of the United States Government. Neither the United States Government nor any agency thereof, nor any of their employees, nor any of their contractors, subcontractors or their employees, makes any warranty, express or implied, or assumes any legal liability or responsibility for the accuracy, completeness, or any third party's use or the results of such use of any information, apparatus, product, or process disclosed, or represents that its use would not infringe privately owned rights. Reference herein to any specific commercial product, process, or service by trade name, trademark, manufacturer, or otherwise, does not necessarily constitute or imply its endorsement, recommendation, or favoring by the United States Government or any agency thereof or its contractors or subcontractors. The views and opinions of authors expressed herein do not necessarily state or reflect those of the United States Government or any agency thereof.

# The Physics and Properties of Free-Electron Lasers

Samuel Krinsky

*Brookhaven National Laboratory, Upton, NY 11973*

**Abstract.** We present an introduction to the operating principles of free-electron lasers, discussing the amplification process, and the requirements on the electron beam necessary to achieve desired performance.

## INTRODUCTION

In the storage rings of synchrotron radiation facilities, the electrons are radiating incoherently [1,2]. Since there is no multi-particle coherence, the radiated intensity is linearly proportional to the number of electrons  $N_e$ . If the electrons in a beam are spatially bunched on the scale of the radiation wavelength [3,4], coherent radiation with intensity proportional to  $N_e^2$  will be emitted. Since  $N_e$  can be very large, coherent emission offers the potential of greatly enhancing the intensity. The technical challenge is to produce the required bunching on the scale of the radiation wavelength. A task that increases in difficulty as the wavelength is decreased.

To obtain coherent emission at short wavelengths, one must develop methods to bunch the electron beam utilizing the radiation. One approach that has already been successfully applied down to the vacuum ultraviolet is the free electron laser (FEL). The FEL [5] is based on a resonant interaction between an electromagnetic wave and an electron beam traveling along the axis of an undulator magnet. The periodic undulator magnetic field produces a transverse component of the electron velocity that couples the energy of the electron to that of the wave. Under general conditions this coupling will merely result in a shifting of energy back and forth between the electron beam and the radiation. However, in resonance, there can be sustained energy transfer from the electrons to the wave. FELs are reviewed in refs. [6-8].

In designing an FEL, one must decide on the type of electron accelerator to be used: e.g. storage ring [9], room temperature linac [10], or superconducting linac [11]. Storage rings provide very high stability and continuous operation; however, the FEL action perturbs the electron beam, thus limiting performance. The development of photocathode RF electron guns [12,13] has made linacs attractive as drivers for FELs. They can produce high peak current and small normalized emittance. The microbunch pulse length in photo-injectors is typically on the order of 10 ps, and bunch compression can be used to reduce the pulse length down to the vicinity of 100 fs. The macropulse structure in room temperature linacs consists of pulse trains separated

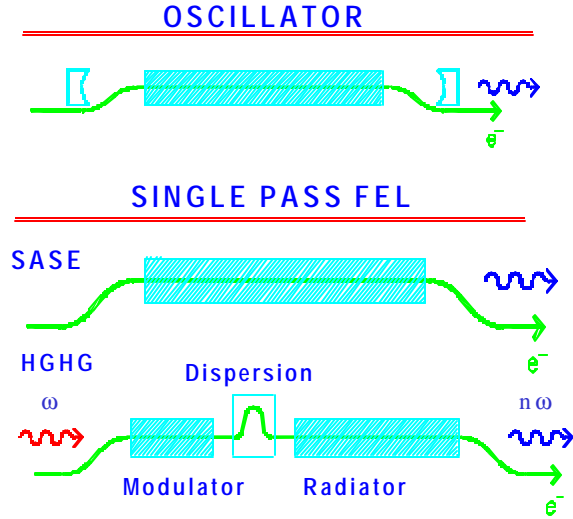


**FIGURE 1.** FEL configurations: oscillator; self-amplified spontaneous-emission; high-gain harmonic generation.

by dead time. Superconducting linacs can provide continuous-wave beams and very high stability.

A fundamental consideration in FEL design is whether to use a high-Q optical cavity, or to operate the FEL as a high-gain single-pass amplifier (see Fig. 1). An optical cavity has many advantages: it requires less gain per pass, simplifying the undulator, and it facilitates the production of narrow bandwidth output radiation. However, it is difficult to utilize optical cavities at short wavelengths because one requires high quality mirrors resistant to radiation damage. For this reason, present effort in the design of short wavelength FELs, from the VUV down to hard x-rays, is predominantly focused on using single pass FEL amplifiers employing long undulators [10].

## UNDULATOR RADIATION

Let us begin our discussion by considering an electron traversing an undulator magnet [1,2,14]. For the purposes of illustrating the basic principles, it is convenient for us to consider the undulator to be helical, resulting in a constant longitudinal velocity (along the undulator axis, z-direction)

$$v^* = c \left( 1 - \frac{1 + K^2}{2g^2} \right). \quad (1)$$

The transverse velocity is

$$\vec{v}_T = -\frac{K}{g} c \left( \hat{x} \cos k_w z + \hat{y} \sin k_w z \right). \quad (2)$$

Here,  $g mc^2$  is the electron energy and  $K$  is the magnetic strength parameter,

$$K \cong 0.93 B_w(T) I_w(cm), \quad (3)$$

where  $B_w$  is the amplitude of the helical undulator field and  $I_w = 2p/k_w$  is the undulator period length.

Consider a wave front radiated in the forward direction. After a time interval  $I_w/v^*$ , the electron has passed through one additional undulator period, and a second wavefront emitted at this time follows the first by a time interval

$$T_s = \frac{I_w}{v^*} - \frac{I_w}{c}, \quad (4)$$

as illustrated in Fig. 2. In the forward direction the radiation spectrum is peaked at wavelength  $I_s = cT_s$ , i.e.

$$I_s = \frac{I_w}{2g^2} (1 + K^2). \quad (5)$$

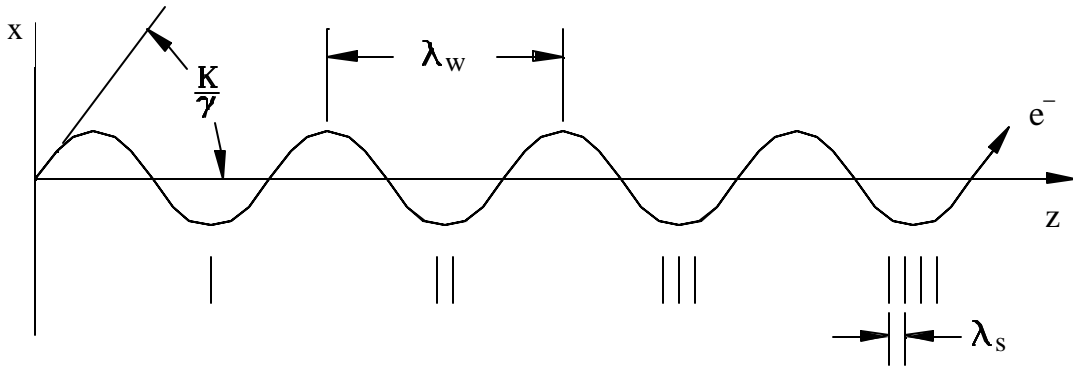


**FIGURE 2.** As the electron traverses successive undulator periods, additional radiation wavefronts are emitted. Since the electron is traveling almost at the speed of light, the electron slips only slightly behind the wavefronts emitted previously. Therefore, the radiation wavelength is much shorter than the undulator period.

For radiation propagating at a polar angle  $J$  relative to the  $z$  axis, the spatial separation of wavefronts emitted before and after an electron has traversed one period of the undulator is

$$I_s(\mathbf{J}) = \frac{I_w}{2g^2} (1 + K^2 + g^2 J^2). \quad (6)$$

In an undulator with  $N_w$  periods, the radiated pulse from one electron has a pulse length of  $N_w I_s$ . Consequently, the line width at fixed observation angle is

$$\frac{\Delta I}{I_s} \cong \frac{1}{N_w}. \quad (7)$$

From Eq. (6), we see that the spectral broadening due to accepting radiation in a cone of half-angle  $\Delta \mathbf{J}$  about the forward direction is  $\Delta I / I_s = g^2 (\Delta \mathbf{J})^2 / (1 + K^2)$ . This broadening will be small only if  $\Delta \mathbf{J} < \mathbf{J}_w$ , where we define

$$\mathbf{J}_w \equiv \sqrt{\frac{1 + K^2}{2N_w g^2}} = \sqrt{\frac{I_s}{L_w}}, \quad (8)$$

with  $L_w = N_w I_w$ . Angle  $\mathbf{J}_w$  characterizes the central cone of the undulator radiation. The power per unit solid angle per unit frequency emitted in the forward direction at  $\mathbf{w} = \mathbf{w}_s = 2\mathbf{p}c / I_s$  by an electron beam of energy  $g$  and current  $I_e$  traversing  $N_w$  periods is given by [1] (mks units, Alfven current  $I_A = 4\mathbf{p}e_o mc^3 / e \cong 17,000 \text{ Amp}$ )

$$\left[ \frac{dP}{d\mathbf{w}d\Omega} \right]_{N_w}^{SPONT} = mc^2 N_w^2 \frac{I_w}{I_s} J, \quad J = \frac{K^2}{1 + K^2} \frac{I_e}{I_A}. \quad (9)$$

## FREE-ELECTRON LASER: LOW-GAIN REGIME

Let us now consider an electron passing through an undulator with longitudinal and transverse velocities as specified in Eqs. (1) and (2). Suppose the electron to be interacting with a co-propagating electromagnetic wave with electric field ( $\mathbf{w}_s = ck_s$ )

$$\vec{E} = E_o \left[ \hat{x} \cos(k_s z - \mathbf{w}_s t + \mathbf{f}) - \hat{y} \sin(k_s z - \mathbf{w}_s t + \mathbf{f}) \right]. \quad (10)$$

The energy transfer between the electron and wave is described by [6-8]

$$\frac{d\mathbf{g}}{dz} = \frac{e}{\mathbf{g} mc^3} \vec{v} \circ \vec{E} = -\frac{eKE_0}{mc^2 \mathbf{g}} \cos(\mathbf{z}(z) + \mathbf{f}), \quad (11)$$

where the ponderomotive phase is

$$\mathbf{z}(z) \equiv (k_s + k_w)z - \mathbf{w}_s t(z). \quad (12)$$

Here,  $t(z)$  is the time of arrival of the electron at position  $z$  along the undulator axis. Differentiating Eq. (12), we find

$$\frac{d\mathbf{z}}{dz} = k_s + k_w - \frac{\mathbf{w}_s}{v^*} \quad (13)$$

The condition for resonance is

$$\frac{d\mathbf{z}}{dz} = 0 \rightarrow v^* = \frac{\mathbf{w}_s}{k_s + k_w} \rightarrow (c - v^*) \frac{I_w}{v^*} = I_s. \quad (14)$$

The resonance condition requires that while traveling through one period of the undulator, an electron falls one radiation wavelength behind the wave, as illustrated in Fig. 3. In resonance, the phase relation that exists between the electron and wave in one period is repeated in subsequent periods making possible a sustained energy transfer.

The resonant energy  $\mathbf{g}_r$  is determined by

$$\frac{1 + K^2}{2\mathbf{g}_r^2} I_w = I_s. \quad (15)$$

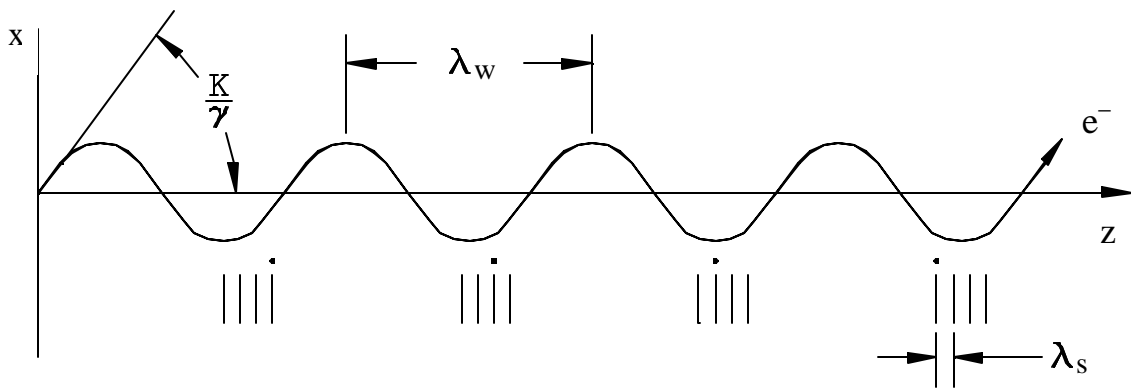


**FIGURE 3.** Resonance condition: as the electron and wave propagate along the axis of the undulator, the electron slips one radiation wavelength behind the wave for each undulator period traversed.

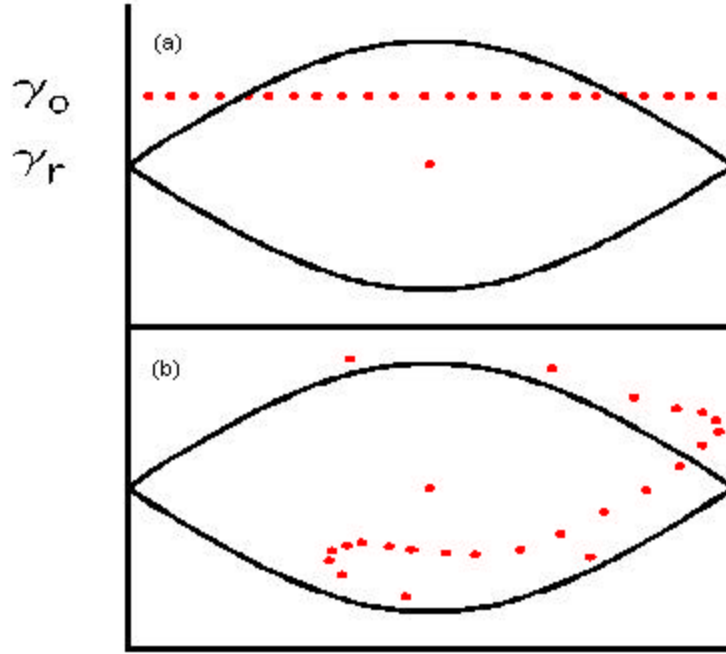


**FIGURE 4.** We show the longitudinal  $z, \mathbf{g}$ -phase space for an electron beam (a) initially monoenergetic and uniformly distributed in phase, and (b) after experiencing a small net energy loss to a co-propagating electromagnetic wave.

When  $\left| \frac{\mathbf{g} - \mathbf{g}_r}{\mathbf{g}_r} \right| \ll 1$ , the equations describing the electron motion become

$$\frac{d\mathbf{z}}{dz} = 2k_w \frac{\mathbf{g} - \mathbf{g}_r}{\mathbf{g}_r} \quad (16)$$

$$\frac{d\mathbf{g}}{dz} = -\frac{eKE_o}{mc^2 \mathbf{g}_r} \cos(\mathbf{z}(z) + \mathbf{f}), \quad (17)$$

If the undulator parameters  $K$  and  $k_w$  are constant, and we ignore the variation of  $E_0$  and  $\mathbf{f}$ , then the ponderomotive phase is determined by the pendulum equation

$$\frac{d^2\mathbf{z}}{dz^2} + \Omega_p^2 \cos(\mathbf{z} + \mathbf{f}) = 0, \quad (18)$$

with



$$\Omega_p^2 = \frac{2ek_w KE_0}{mc^2 g_r^2}. \quad (19)$$

This is an appropriate description in the low-gain regime, when amplification of the wave in a single pass through the undulator is small. For an electron beam which is initially monoenergetic and uniformly distributed in phase, an illustration of net energy loss by the electron beam to the radiation is presented in Fig. 4.

When the gain per pass is small, a large total gain can be achieved by placing the undulator between the mirrors of an optical resonator. If the electron beam is comprised of a long train of bunches, with neighboring bunches space by twice the length of the optical cavity, the radiation can be repeatedly amplified as it interacts with successive bunches.

## **FREE-ELECTRON LASER: HIGH-GAIN REGIME**

It is difficult to use optical cavities at short wavelengths because of the need for high-quality mirrors resistant to radiation damage. Therefore, to generate short wavelength radiation, high-gain single pass amplifiers employing long undulators are of interest. The mathematical description of high-gain amplifiers [6-8, 15-17] must take into account the variation of the radiation field. High gain results from a collective instability leading to exponential growth of the radiated power,

$$P \propto \exp(z/L_G), \quad (20)$$

where  $L_G$  is the e-folding or gain length (see Fig. 5).

The mechanism leading to exponential growth is as follows: Electrons gain or lose energy depending upon their phase  $z$  with respect to the electromagnetic wave. The resulting energy modulation of the electron beam gives rise to a spatial bunching due to the dispersion in the undulator (i.e.  $v^*$  larger for higher-energy electrons). The density modulation at the radiation wavelength then produces enhanced coherent emission, amplifying the radiation intensity. The positive feedback loop is closed since the increase in radiation intensity enhances the energy modulation of the electron beam.

Suppose the electron beam entering the undulator is initially monoenergetic with energy  $g_0$ , and uniformly distributed in phase, and there exists a small coherent laser seed. An illustration [7] of the evolution of the electron beam's longitudinal phase space distribution and the corresponding increase of the radiation field amplitude is presented in Fig. 6.

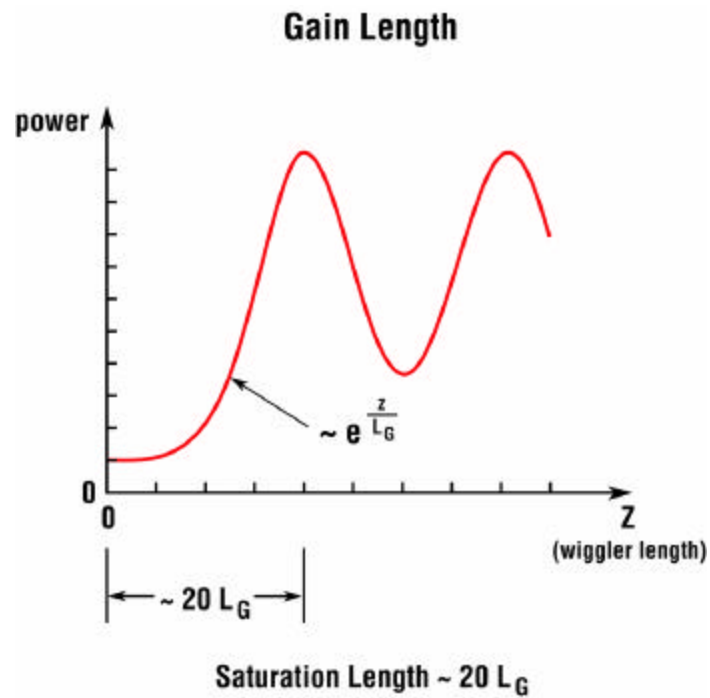


**FIGURE 5.** The radiated power increases exponentially until the instability saturates. In the case of self-amplified spontaneous-emission, the amplifier starts-up from shot noise, and it takes about 20 power gain-lengths to reach saturation.

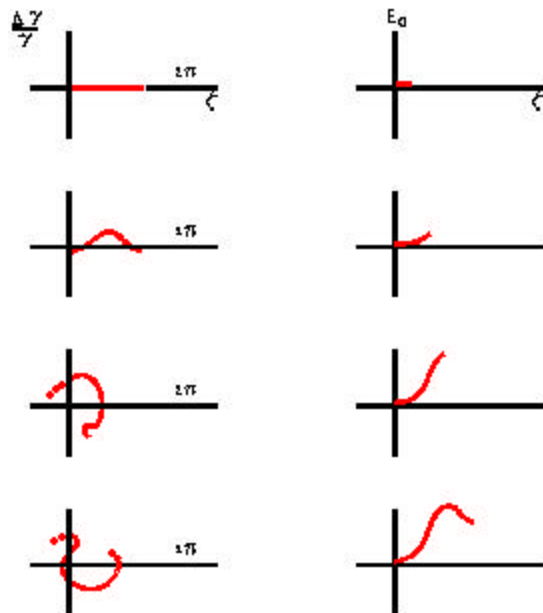


**FIGURE 6.** Evolution of the longitudinal phase space of the electron beam, initially monoenergetic and uniformly distributed in phase, and of the amplitude of the radiation field which starts at a small non-vanishing value.

As the radiation intensity increases, the “pendulum frequency,”  $\Omega_p$  [Eq. (19)], becomes larger. The exponential process saturates when the frequency of rotation in the phase space bucket becomes comparable to the growth rate:

$$\Omega_p \cong \frac{1}{L_G}. \quad (21)$$

Within the one-dimensional approximation, in which dependence on transverse coordinates is ignored, the growth rate can be written in the form,

$$\frac{1}{L_G} = \sqrt{3} \, 2\mathbf{r} \, k_w, \quad (22)$$

where the dimensionless Pierce parameter  $\mathbf{r}$  is given by [17]

$$(2\mathbf{r})^3 = \frac{I_s I_w}{p A g_o} \frac{J}{g_o}. \quad (23)$$

The scaled current  $J$  was defined in Eq. (9) and  $A$ =cross-sectional area of electron beam. Using Eqs. (19), (22) and (23) in Eq. (21), one finds that the saturated radiation power is approximately given by

$$P_{sat} \cong \mathbf{r} E_e (GeV) I_e (Amp), \quad (24)$$

where  $E_e$ (GeV) is the electron energy in GeV and  $I_e$ (Amp) is the electron current in Amperes. We see that the Pierce parameter determines the gain length via Eq. (22) and the efficiency with which the exponential gain process can extract energy from the electron beam and give it to the radiation via Eq. (24).

## One-Dimensional Theory

We shall present a brief introduction to the one-dimensional theory (neglecting dependence on transverse coordinates) of the FEL in the linear regime before saturation [15-17]. Consider the electron beam at the undulator entrance to be monoenergetic,  $\mathbf{g} = \mathbf{g}_o$ , and uniformly distributed in phase, with  $n_1$  electrons per unit length. Define,

$$\mathbf{t} = k_w z, \quad \mathbf{z} = (k_s + k_w)z - \mathbf{w}_s t, \quad (25)$$

where  $k_s = \mathbf{w}_s / c = 2\mathbf{g}_0^2 k_w / (1 + K^2)$ . Introduce the line density  $\Lambda(\mathbf{z}, \mathbf{t}) \equiv$  the number of electrons per unit length, and the energy deviation  $p(\mathbf{z}, \mathbf{t}) \equiv 2(\mathbf{g}(\mathbf{z}, \mathbf{t}) - \mathbf{g}_o) / \mathbf{g}_o$ , and write the radiated electric field in the form

$$\vec{E} = \text{Re} \left[ (\hat{x} + i \hat{y}) E e^{i(k_s z - \mathbf{w}_s \mathbf{t})} \right]. \quad (26)$$

The slowly varying complex amplitude  $E \equiv E_o e^{i\mathbf{f}}$  [see Eq. (10)].

Let us suppose the line density, energy deviation and the electric field amplitude have small sinusoidal perturbations:

$$\Lambda(\mathbf{z}, \mathbf{t}) \equiv n_1 + \Lambda_q(\mathbf{t}) e^{i(1+q)\mathbf{z}}, \quad (27)$$

$$p(\mathbf{z}, \mathbf{t}) \equiv p_q(\mathbf{z}, \mathbf{t}) e^{i(1+q)\mathbf{z}}, \quad (28)$$

$$E(\mathbf{z}, \mathbf{t}) \equiv E_q(\mathbf{t}) e^{iq\mathbf{z}}, \quad (29)$$

where  $q = (\mathbf{w} - \mathbf{w}_s) / \mathbf{w}_s$  is the frequency detuning. We keep only terms linear in the perturbations. The variation in the electron energy deviation due to the radiated electric field is described by Eq. (11). Neglecting the non-resonant  $E_q^*$  term, one finds

$$\frac{\partial p_q}{\partial \mathbf{t}} = -\frac{2d_2}{\mathbf{g}_o^2} E_q. \quad (30)$$

The change in the density modulation resulting from the energy modulation of the electron beam is given by the equation of continuity  $[\partial \Lambda / \partial \mathbf{t} + \partial(p\Lambda) / \partial \mathbf{z} = 0]$ . Linearizing, one derives

$$\frac{\partial \Lambda_q}{\partial \mathbf{t}} = -i(1+q)n_1 p_q. \quad (31)$$

The increment in the electric field driven by the density modulation is determined by the one-dimensional paraxial wave equation

$$\left( \frac{\partial}{\partial \mathbf{t}} + iq \right) E_q = \frac{d_1}{\mathbf{g}_o} \Lambda_q, \quad (32)$$

where (mks units)

$$d_1 = \frac{eK}{2k_w A \mathbf{e}_o}, \quad d_2 = \frac{eK}{2k_w mc^2}, \quad (33)$$

and  $A$  is the cross-sectional area of the electron beam. Eqs. (30), (31) and (32) imply

$$\frac{\partial^2}{\partial \mathbf{t}^2} \left( \frac{\partial}{\partial \mathbf{t}} + iq \right) E_q = i(1+q)(2\mathbf{r})^3 E_q, \quad (34)$$

with  $(2\mathbf{r})^3 = 2d_1 d_2 n_1 / \mathbf{g}_o^3$ , the Pierce parameter introduced in Eq. (23).

The solution to Eq. (34) has the form

$$E_q(\mathbf{t}) = a_1 e^{s_1 \mathbf{t}} + a_2 e^{s_2 \mathbf{t}} + a_3 e^{s_3 \mathbf{t}} \quad (35)$$

where the coefficients  $a_1, a_2, a_3$  are determined from the initial conditions  $E_q(0), \Lambda_q(0)$ , and  $p_q(0) = 0$ . The Laplace transform parameters  $s_1, s_2, s_3$  are the solutions of the cubic dispersion relation

$$s^2(s+iq) = i(2\mathbf{r})^3. \quad (36)$$

A useful approximation is

$$s \cong 2\mathbf{r} \left[ \mathbf{m} - \frac{i}{3} \left( \frac{q}{2\mathbf{r}} \right) - \frac{1}{9\mathbf{m}} \left( \frac{q}{2\mathbf{r}} \right)^2 \right]. \quad (37)$$

There are three modes: growing; decaying and oscillating; corresponding to  $\mathbf{m} = \frac{\sqrt{3}}{2} + \frac{i}{2}, -\frac{\sqrt{3}}{2} + \frac{i}{2}, -i$ . For the exponentially growing mode,

$$\text{Re } s_1 \cong (2\mathbf{r}) \frac{\sqrt{3}}{2} \left[ 1 - \frac{1}{9} \left( \frac{q}{2\mathbf{r}} \right)^2 \right]. \quad (38)$$

It can now be shown that the evolution of the electric field is determined by [18-19,23]

$$E_q(\mathbf{t}) = H_q^{(2)}(\mathbf{t}) E_q(0) + H_q^{(1)}(\mathbf{t}) \frac{d_1}{\mathbf{g}_o} \Lambda_q(0), \quad (39)$$

where the transfer functions are given by (m=1,2)

$$H_q^{(m)}(\mathbf{t}) = \frac{s_1^m e^{s_1 \mathbf{t}}}{(s_1 - s_2)(s_1 - s_3)} + \frac{s_2^m e^{s_2 \mathbf{t}}}{(s_2 - s_3)(s_2 - s_1)} + \frac{s_3^m e^{s_3 \mathbf{t}}}{(s_3 - s_1)(s_3 - s_2)}. \quad (40)$$

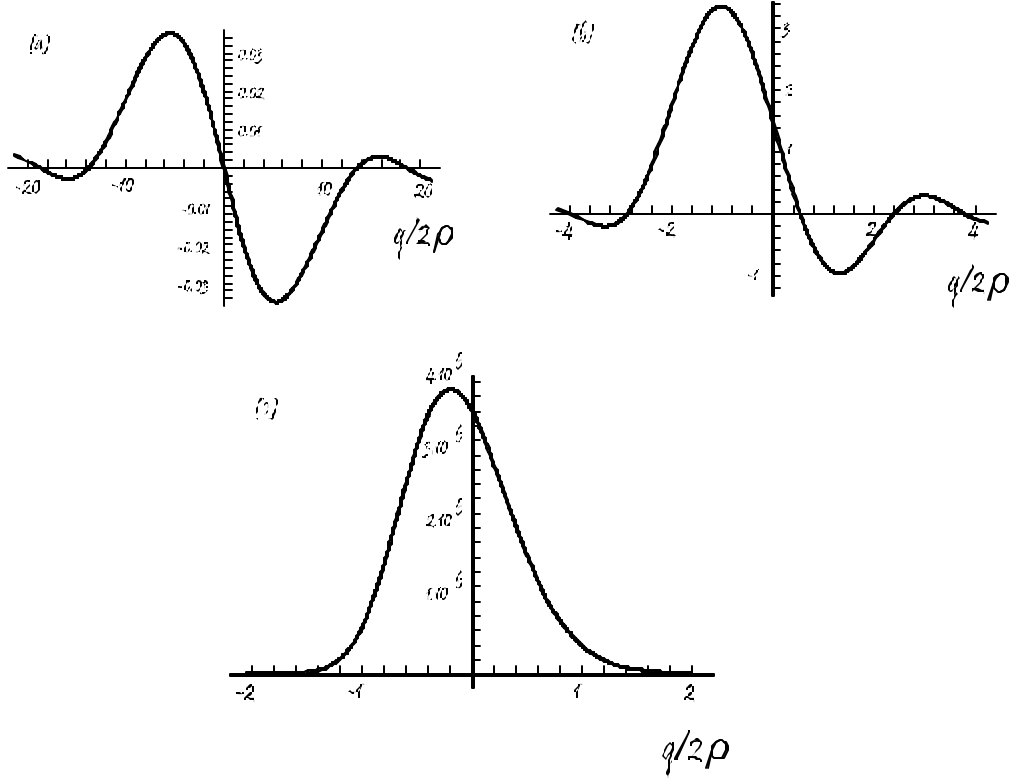


**FIGURE 7.** Plot of  $|H_q^{(2)}(k_w z)|^2 - 1$  versus  $q/2r$ , for: (a)  $2rk_w z = 0.5$ ; (b)  $2rk_w z = 1.0$ ; (c)  $2rk_w z = 10$ . For low gain (a), the interference of the three modes is important. In the high-gain regime (c), the growing mode dominates.

In the exponential-gain regime the growing mode dominates (see Fig. 7) and

$$|H_q^{(m)}(t)|^2 \cong \frac{1}{9} (2r)^{2m-4} e^{-q^2 w_s^2 / 2s_w^2} e^{z/L_G}. \quad (41)$$

The power gain length,  $L_G$ , has the value given in Eq. (22), and the gain bandwidth is

$$s_w = w_s \sqrt{\frac{3\sqrt{3} r}{t}}. \quad (42)$$

### Self-Amplified Spontaneous-Emission (SASE)

In the absence of an external seed laser,  $E_q(0) = 0$ , so the FEL amplifier starts up from the shot noise in the electron beam [18-23],

$$\Lambda_q(0) = \frac{k_s}{2\mathbf{p}} \sum_j e^{i(1+q)\mathbf{w}_s t_j(0)}. \quad (43)$$

Here, the sum is over the electrons comprising the beam and  $t_j(0)$  is the arrival time of the  $j^{\text{th}}$  electron at the undulator entrance. It follows from Eq. (39), that

$$E_q(\mathbf{t}) = H_q^{(1)}(\mathbf{t}) \frac{d_1 k_s}{\mathbf{g}_o} \frac{1}{2\mathbf{p}} \sum_j e^{i(1+q)\mathbf{w}_s t_j(0)}. \quad (44)$$

We can treat the arrival times  $t_j(0)$  as independent random variables. Therefore, at a fixed position,  $\mathbf{t} = k_w z$ , along the undulator,  $E_q(\mathbf{t})$  and its Fourier transform  $E(\mathbf{t}, \mathbf{z})$  are sums of independent random terms. It follows from the Central Limit Theorem [24] that the probability distribution describing the spectral intensity  $I \propto |E_q|^2$ , or the time-domain intensity  $I \propto |E|^2$ , is the negative exponential distribution

$$p_I(I) = \frac{1}{\langle I \rangle} e^{-I/\langle I \rangle}. \quad (45)$$

The intensity fluctuation is 100%.

The output intensity as a function of time exhibits spiking [25] (see Fig. 8), and the width of the intensity peaks are characterized by the coherence time [24,26]  $T_{coh} = \sqrt{\mathbf{p}} / \mathbf{s}_w$ . The spectral intensity also exhibits spikes (Fig. 9), and their widths are inversely proportional to the electron bunch duration  $T_b$ .

Let us consider the energy in a single SASE pulse,

$$W(\mathbf{t}) \propto \int_0^{\mathbf{w}_s T_b} |E(\mathbf{z}, \mathbf{t})|^2 dz. \quad (46)$$

For fixed  $\mathbf{t}$ , the pulse can be divided up into  $M$  statistically independent time-intervals of width  $T_{coh}$ . The fluctuation within a single coherent region is 100%, but the fluctuations  $\mathbf{s}_w$  of the energy in the entire pulse is reduced and given by [24,26]

$$\mathbf{s}_w^2 = \frac{(W - \langle W \rangle)^2}{\langle W \rangle^2} = \frac{1}{M} = \frac{T_{coh}}{T_b}. \quad (47)$$

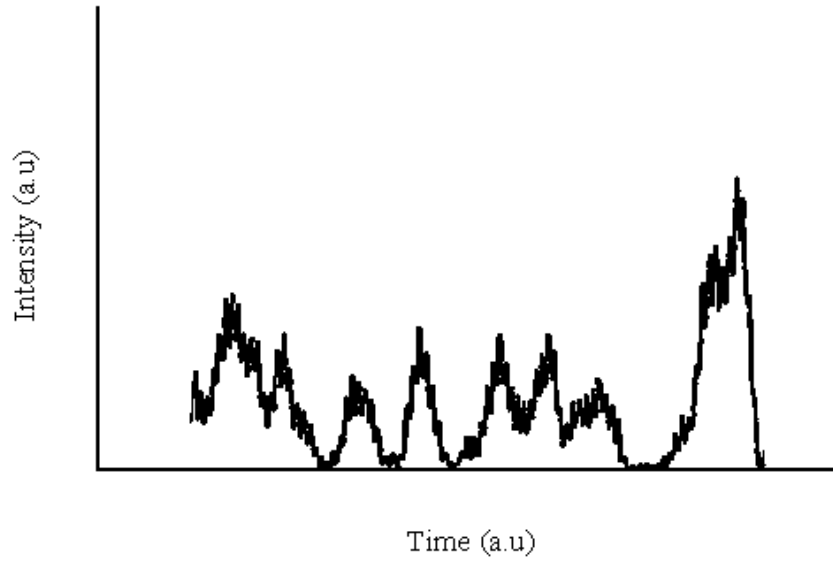


**FIGURE 8.** Intensity spiking in the time-domain. The width of the peaks is characterized by the SASE coherence time  $T_{coh} = \sqrt{p} / s_w$ .

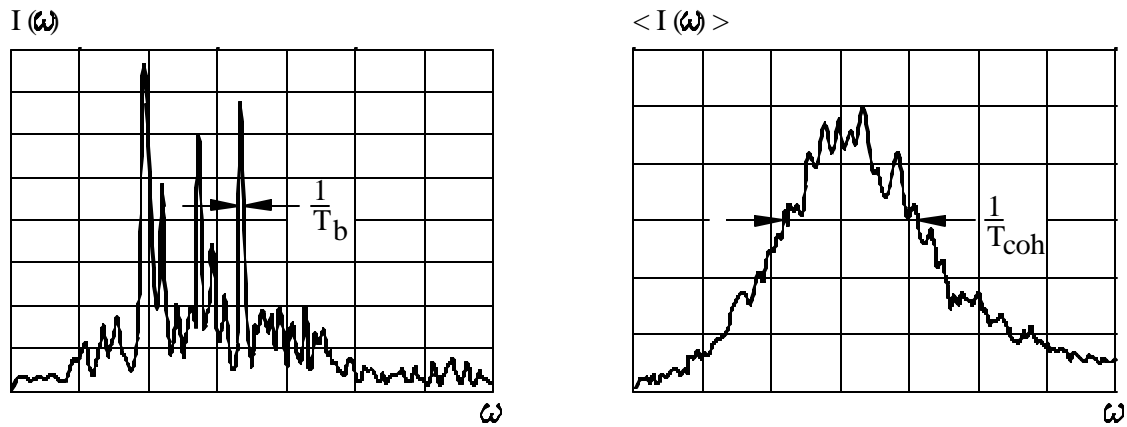


**FIGURE 9.** Intensity spiking in the frequency-domain. In the single-shot spectrum shown on the left, the width of the peaks is inversely proportional to the electron bunch duration  $T_b$ . The average of many SASE pulses is illustrated on the right, and in this case the width is proportional to the gain bandwidth  $s_w = \sqrt{p} / T_{coh}$ .



The energy per pulse is described by the gamma distribution [24],

$$p_W(W) = \frac{M^M}{\Gamma(M)} \left( \frac{W}{\langle W \rangle} \right)^{M-1} \frac{1}{\langle W \rangle} \exp\left(-M \frac{W}{\langle W \rangle}\right). \quad (48)$$

It follows from Eqs. (41) and (44) that the average output SASE power spectrum can be expressed in the form [20]

$$\frac{dP}{d\mathbf{w}} = \left[ \left( \frac{dP}{d\mathbf{w}} \right)_{Input} + \left( \frac{dP}{d\mathbf{w}} \right)_{Noise}^{1-D} \right] \frac{1}{9} e^{-(\mathbf{w}-\mathbf{w}_s)^2 / 2\mathbf{s}_w^2} e^{z/L_G}, \quad (49)$$

where

$$\left( \frac{dP}{d\mathbf{w}} \right)_{Noise}^{1-D} = \frac{\mathbf{r} \mathbf{g}_o m c^2}{2\mathbf{p}}, \quad (50)$$

arises from the shot noise in the electron beam and  $(dP/d\mathbf{w})_{Input}$  represents an input laser seed. In the case of SASE (no seed), the average output power is [18,19]

$$P = \frac{1}{9} \frac{P_{sat}}{\sqrt{2N_{coh}}} e^{z/L_G}. \quad (51)$$

$P_{sat}$  is the saturation power defined in Eq. (24) and  $N_{coh} = n_1 c T_{coh}$  is the number of electrons in a coherence length. Typically,  $N_{coh}$  is large, and it takes about 20 SASE gain lengths to reach saturation (Fig. 5).

The noise (within the one-dimensional approximation) amplified in SASE is the spontaneous undulator radiation with frequency  $\mathbf{w} = \mathbf{w}_s$  emitted in the first two power gain lengths into a cone of solid angle  $I_s^2 / A$  about the forward direction ( $A$  being the cross-sectional area of the electron beam). This follows from observing that [22]

$$\left( \frac{dP}{d\mathbf{w}} \right)_{Noise}^{1-D} = \frac{3}{4} \frac{I_s^2}{A} \left( \frac{dP}{d\mathbf{w} d\Omega} \right)_{N_w=2L_G / I_w}^{SPONT}, \quad (52)$$

which can be verified from Eqs. (9), (22) and (23).

## Constraints On Electron Beam Quality

To achieve high gain, the resonant condition must hold for most electrons. This imposes tolerances on the energy spread and emittance. One should note that, as illustrated in Fig. 2, since the electrons are traveling almost at the speed of light, the radiation emitted by an electron moves ahead of it by only one radiation wavelength for each undulator period traversed. Therefore, an electron can influence only those electrons less than one slippage distance,  $N_w \mathbf{l}_s$  in front of it. Tolerances to assure desired gain restrict the properties of the electron beam within a slice shorter than one slippage distance. To assure the entire electron beam contributes, tolerances must be imposed on the entire beam.

Recall from Eq. (15), that the resonance condition is

$$\frac{1+K^2}{2\mathbf{g}_r^2} \mathbf{l}_w = \mathbf{l}_s. \quad (53)$$

Suppose an electron has energy  $\mathbf{g} = \mathbf{g}_r + \mathbf{d} \mathbf{g}$ . In this case, while traversing one undulator period, the electron slips a distance  $\mathbf{l}_s + \mathbf{d} \ell$  behind the wave:

$$\frac{1+K^2}{2\mathbf{g}^2} \mathbf{l}_w = \mathbf{l}_s + \mathbf{d} \ell, \quad (54)$$

where

$$\mathbf{d} \ell \cong -2\mathbf{l}_s \frac{\mathbf{d} \mathbf{g}}{\mathbf{g}_r}. \quad (55)$$

Let us assume that in order to maintain coherent energy transfer over a section of undulator of length  $2L_G$ , it is necessary that

$$|\mathbf{d} \ell| < \frac{\mathbf{l}_s}{4N_G}, \quad (56)$$

where  $N_G = 2L_G / \mathbf{l}_w$  is the number of undulator periods in two power gain lengths. The significance of the tolerance imposed in Eq. (56) is that no electron will fall more than  $90^\circ$  out of phase with the wave while traversing two power gain lengths. From Eqs. (55) and (56), we see that the tolerance on the energy spread is

$$\left| \frac{\mathbf{d} \mathbf{g}}{\mathbf{g}_r} \right| < \frac{1}{8N_G}. \quad (57)$$

Now consider an electron that has the resonant energy  $\mathbf{g}_r$ , but which is traveling at a small angle  $\mathbf{J}$  relative to the  $z$ -direction. Since such an electron must travel a longer distance to traverse one undulator period, it slips a distance  $\mathbf{l}_s + \mathbf{d} \ell$  behind the wave:

$$\left( \frac{1+K^2}{2\mathbf{g}_r^2} + \frac{\mathbf{J}^2}{2} \right) \mathbf{l}_w \cong \mathbf{l}_s + \mathbf{d} \ell, \quad (58)$$

where

$$\mathbf{d} \ell = \frac{\mathbf{J}^2}{2} \mathbf{l}_w. \quad (59)$$

To assure coherent transfer of energy from the electron beam to the wave over two power gain lengths, we again impose the constraint of Eq. (53), resulting in the tolerance

$$\mathbf{J} < \sqrt{\frac{\mathbf{l}_s}{4L_G}}. \quad (60)$$

In the special case when the horizontal and vertical emittances are equal,  $\mathbf{e}_x = \mathbf{e}_y = \mathbf{e}$ , and the horizontal and vertical betatron functions are equal,  $\mathbf{b}_x = \mathbf{b}_y = \mathbf{b}$ , we can write  $\mathbf{J}^2 = 2\mathbf{e} / \mathbf{b}$  so the inequality (60) can be interpreted as a tolerance on the emittance [27]:

$$\mathbf{e} < \frac{\mathbf{l}_s}{4} \frac{\mathbf{b}}{2L_G}. \quad (61)$$

Diffraction of radiation out of the electron beam can result in a reduction of gain. The loss of gain [28,21] should be small as long as the Rayleigh range corresponding to the transverse dimensions of the electron beam is long compared to the gain length. For a cylindrical electron beam of radius  $R = \sqrt{\mathbf{b} \mathbf{e}}$ , we can write this condition as

$$k_s \mathbf{b} \mathbf{e} > 2L_G. \quad (62)$$

In order to satisfy both Eqs. (61) and (62), we should have  $\mathbf{b} > 2L_G$ . Since the gain is larger for higher electron density, the optimum will be near  $\mathbf{b} \cong 2L_G$ .

In the linear regime before saturation, the coupled Vlasov-Maxwell equations have been used to derive a dispersion relation incorporating the effects of the energy spread,

emittance, and focusing of the electron beam and the diffraction and guiding of the radiation. The gain length was expressed in the scaled form<sup>1</sup> [29]:

$$\frac{1}{2L_G} = \frac{2p}{I_w} D G \left( \frac{4pe}{I_s}, \frac{s_g}{D}, \frac{I_w}{DI_b}, \frac{w-w_s}{w_s D} \right). \quad (63)$$

with

$$D = 4 \left( \frac{J}{g_o} \right)^{1/2}. \quad (64)$$

Here, the scaled current J was defined in Eq. (9),  $s_g$  is the fractional energy spread and  $I_b = 2p b$  the betatron wavelength. The scaling function G can be calculated very accurately [29] and the results agree with computer simulations to within 5-10%. This work was later extended in refs. [30-32]. The analytic determination of the gain length makes possible rapid computation, and facilitates FEL design optimization.

Let us now briefly discuss the dependence of the FEL parameters on output wavelength  $I_s$ . As we reduce  $I_s$ , the required transverse emittance  $\epsilon$ , as estimated in Eq. (61), decreases proportionally. Thus, for a given normalized emittance,  $e_n \equiv g e$ , the required energy increases. As the energy is increased, the current must also be increased to prevent the scaling parameter D [Eq. (64)] from becoming too small. Once the energy and wavelength are determined, the undulator period  $\lambda_w$  and field strength parameter K must be chosen to satisfy the resonance condition of Eq. (5), as well as certain practical and economic constraints. In particular, as one decreases the period, one must also decrease the magnet gap to prevent the field strength parameter from becoming too small. Therefore, the vertical aperture required for the electron beam, and perhaps electron beam diagnostics, limits how small the period can be

---

<sup>1</sup> When the electron beam size is large enough and the angular spread and energy spread are small, the gain length given in Eq. (63) approaches the result of 1-D theory, Eq. (22). In this regime,

$$G \left( \frac{4pe}{I_s}, 0, \frac{I_w}{DI_b}, 0 \right) \cong k \left( \frac{I_s}{4pe} \frac{I_w}{DI_b} \right)^{1/3},$$

with

$$k = \frac{\sqrt{3}}{2} \left( \frac{pb e}{2A} \right)^{1/3}.$$

The area of the electron beam  $A = n_b/n_1$ , where  $n_b$  is the peak value (at  $R=0$ ) of the number of electrons per unit volume and  $n_1$  is the number of electrons per unit length. For the parabolic transverse distribution, considered in [29],  $A = 3pb e$  and  $k \cong .477$ .

made. Also, the magnet period must not be made too long, or else the size and cost of the system will become unnecessarily large.

In this paper, we have confined our attention to the fundamental frequency. However, near saturation, significant intensity is produced at the low harmonics of the fundamental. We refer the reader to the literature to pursue this interesting subject [33-36].

### Some Recent Experiments on FEL Amplifiers

In Table 1, we present some of the fundamental parameters for four proof-of-principle SASE experiments which have been carried out over the last few years in the visible and vacuum ultraviolet: TTF1 at DESY [37]; LEUTL at ANL [38]; VISA at BNL [39]; and DUV-FEL at BNL [40]. The parameters correspond to reported experiments and do not necessarily represent the best or shortest wavelength performance achieved to-date. In the last column, we give the parameters for the design of the LCLS at SLAC [10]. Saturation of the SASE process has been observed at 95 nm at TTF1, at 130 nm at LEUTL and 800 nm at VISA. Agreement obtained between the experimental results and theory provides a firm foundation for the development of future x-ray facilities based on FEL amplifiers. The key challenge is to produce and transport the required high-brightness electron beams.

Table. 1. Parameters for FEL Projects

	TTF1	LEUTL	VISA	DUV-FEL	LCLS
$I_s$ (nm)	95	530	800	400	0.15
$E_e$ (MeV)	250	217	72.6	140	14,300
$I_w$ (mm)	27	33	18	39	30
$K$	1.2	3.1	1.26	1.1	3.7
$ge$ (mm)	6	8.5	2	6	1.2
$b_{av}$ (m)	1.2	1.4	0.27	3.2	7
$I_e$ (Amp)	1300	266	200	500	3400
$L_G$ (m)	0.67	0.57	0.17	0.68	4.7

The SASE FEL can generate high-intensity radiation with good transverse coherence but limited temporal coherence. Consideration has been given to seeding the FEL amplifier to improve temporal coherence. If a low power laser exists at the wavelength of interest, then the FEL can be used to amplify the signal to high power. In the cases of greatest interest, no such seed is available. However, one can use a seed at a longer wavelength and carry out harmonic generation in the FEL amplifier to generate temporally coherent short wavelength output. A proof-of-principle experiment of such a high-gain harmonic-generation (HG) FEL was successfully carried out in the infrared [41]. The DUV-FEL is designed to continue investigation of HG in the visible and vacuum ultraviolet. Another approach to seeding a short wavelength FEL consists of installing a monochromator after an initial section of

undulator, and then amplifying the output in a second undulator [42]. A variant of this approach is the regenerative amplifier [43], in which the undulator is placed in a low-Q optical cavity whose reflectors consist of a mirror and a grating. The radiation from earlier bunches provide the monochromatized seed for the later bunches.

In SASE, the output pulse duration is determined by the density profile of the electron bunch. There is a strong desire to produce radiation pulses of femtosecond duration, which is generally shorter than the electron bunch. One possibility is to provide a short seed in an HGHG FEL. Another approach is to put an energy chirp on the electron bunch - producing a frequency chirp of the output radiation. A monochromator can then be used to select a short slice of the pulse [44]. Improvement of the output of an FEL amplifier is currently an active area of research, and many other schemes are currently under investigation.

## ACKNOWLEDGMENTS

I wish to thank Dr. Li-Hua Yu for many illuminating discussions on the physics of free-electron lasers. This work was supported by the Department of Energy, Office of Basic Energy Sciences, under contract No. DE-AC02-98CH10886.

## REFERENCES

1. Krinsky, S., Perlman, M.L., and Watson, R.E., "Characteristics of Synchrotron Radiation and of its Sources" in *Handbook on Synchrotron Radiation*, edited by E.E. Koch, Amsterdam: North-Holland, 1983, pp. 65-171.
2. Kim, K.J., "Characteristics of Synchrotron Radiation" in *Proceedings U.S. Particle Accelerator School-1987*, edited by M. Month et al, AIP Conference Proceedings 184, New York: American Institute of Physics, 1989, pp. 565-632.
3. Nakazato, T. et al, *Phys. Rev. Lett.* **63**, 1245 (1989).
4. Blum, E.B., Happek, U., and Sievers, A.J., *Nucl. Instrum. Methods* **A307**, 568 (1991).
5. Madey, J.M.J., *J. Appl. Phys.* **42**, 1906 (1971).
6. Colson, W.B., in *Laser Handbook*, vol. 6, edited by Colson, W.B. et al, Amsterdam: North-Holland, 1990.
7. Murphy, J.B. and Pellegrini, C., in *Laser Handbook*, vol. 6, edited by Colson, W.B. et al, Amsterdam: North-Holland, 1990.
8. Saldin, E.L., Schneidmiller, E.A., and Yurkov, M.V., *The Physics of Free Electron Lasers*, Berlin: Springer, 2000.
9. Litvinenko, V.N., Park, S.H., Pinayev, I.V., and Wu, Y., *Nucl. Instrum. Methods* **A475**, 195 (2001).
10. Galayda, J., ed., *Linac Coherent Light Source Conceptual Design Report*, SLAC-R-593 (2002).
11. Neil, G.R. et al, *Phys. Rev. Lett.* **84**, 662 (2000).
12. Fraser, J. and Sheffield, R., *Nucl. Instrum. Methods* **A250**, 71 (1986).
13. Wang X., Qiu, X., and Ben-Zvi, I., *Phys. Rev.* **E54**, R3121 (1996).
14. Krinsky, S., *IEEE Trans. Nucl. Sci.* **NS-30**, 3078 (1983).
15. Kroll, N.M. and McMullin, *Phys. Rev.* **A17**, 300 (1978).
16. Debennev, Y.S., Kondratenko, A.M. and Saldin, E.L., *Nucl. Instrum. Methods* **A193**, 415 (1982).
17. Bonifacio, R., Pellegrini, C., and Narducci, L.M., *Opt. Commun.* **50**, 373 (1984).
18. Kim, K.J., *Nucl. Instrum. Methods* **A250**, 396 (1986).
19. Wang, J.M. and Yu, L.H., *Nucl. Instrum. Methods* **A250**, 484 (1986).
20. Kim, K.J., *Phys. Rev. Lett.* **57**, 1871 (1986)
21. Krinsky, S. and Yu, L.H., *Phys. Rev.* **A35**, 3406 (1987).

22. Yu, L.H. and Krinsky, S., *Nucl. Instrum. Methods* **A285**, 119 (1989).
23. Krinsky, S., *Phys. Rev.* **E59**, 1171 (1999).
24. Saldin, E.L., Schneidmiller, E.L. and Yurkov, M.V., *Nucl. Instrum. Methods* **A407**, 291 (1998)
25. Bonifacio, R., De Salvo, L., Pierini, P., Piovella, N., and Pellegrini, C., *Phys. Rev. Lett.* **73**, 70 (1994).
26. Yu, L.H. and Krinsky, S., *Nucl. Instrum. Methods* **A407**, 261 (1998).
27. Yu, L.H. and Krinsky, S., *Nucl. Instrum. Methods* **A272**, 436 (1988).
28. Moore, G.T., *Nucl. Instrum. Methods* **A239**, 19 (1985).
29. Yu, L.H., Krinsky, S., and Gluckstern, R.L., *Phys. Rev. Lett.* **64**, 3011 (1990).
30. Chin, Y.H., Kim, K.J. and Xie, M., *Phys. Rev.* **A46**, 6662 (1992).
31. Xie, M., *Nucl. Instrum. Methods* **A445**, 59 (2000).
32. Huang, Z. and Kim, K.J., *Nucl. Instrum. Methods* **A475**, 59 (2001)
33. Bonifacio, R., De Salvo, L., and Pierini, P., *Nucl. Instrum. Methods* **A293**, 627 (1990).
34. Schmidt, M.J. and Elliott, C.J., *Phys. Rev.* **A34**, 4843 (1986); **A41**, 3853 (1990).
35. Freund, H.P., Biedron, S.G., and Milton, S.V., *IEEE J. Quantum Electron.* **QE-36**, 275 (2000); *Nucl. Instrum. Methods* **A445**, 53 (2000).
36. Huang, Z. and Kim, K.J., *Nucl. Instrum. Methods* **A475**, 112 (2001)..
37. Ayvazyan et al, *Phys. Rev. Lett.* **88**, 104802 (2002).
38. Milton, S.V. et al, *Science* **292**, 2037 (2001).
39. A. Tremaine et al, "Characterization of an 800 nm SASE FEL at Saturation," Proc. FEL2001.
40. A. Doyuran et al, Proc. EPAC 2002.
41. Yu, L.H. et al, *Science* **289**, 932 (2000).
42. Saldin, E.L., Schneidmiller, E.A. and Yurkov, M.V., *Nucl. Instrum. Methods* **A445**, 178 (2000).
43. B. Faatz et al, *Nucl. Instrum. Methods* **A429**, 424 (1999).
44. Schroeder, C.,B. et al, "Chirped Beam Two-Stage SASE-FEL for High-Power Femtosecond Pulse Generation," *Proc. FEL 2001*.